Distinguishing the Direct Radiative, Surface Warming, and Ozone Mediated Contributions to the Acceleration of the Brewer–Dobson Circulation under Abrupt CO_2 Forcing

MOLLY E. MENZEL,[a,b] CLARA ORBE,[a,c] AND LORENZO M. POLVANI[c,d,e]

[a] *NASA Goddard Institute for Space Studies, New York, New York*
[b] *NASA Postdoctoral Program Fellowship, New York, New York*
[c] *Department of Applied Physics and Applied Mathematics, Columbia University, New York, New York*
[d] *Department of Earth and Environmental Sciences, Columbia University, New York, New York*
[e] *Lamont-Doherty Earth Observatory, Palisades, New York*

(Manuscript received 29 August 2025, in final form 7 January 2026, accepted 27 February 2026)

ABSTRACT: The acceleration of the Brewer–Dobson circulation is one of the most robust impacts on the atmospheric circulation of increasing levels of carbon dioxide (CO_2). However, a complete understanding of the mechanisms leading to that acceleration is as yet incomplete. Here, using a single-model framework, we separate and quantify three largely independent pathways that lead to Brewer–Dobson circulation (BDC) acceleration under an abrupt $4 \times CO_2$ forcing: the warming of sea surface temperatures (SSTs), the cooling of the stratosphere from direct radiative forcing, and the composition feedbacks associated with changes of the ozone layer, each of which is caused by increased CO_2. We accomplish this by contrasting NASA Goddard Institute for Space Studies (GISS) model E2.2 simulations in fully coupled and atmosphere-only configurations. First, we validate our methodology and demonstrate that the response in the fully coupled model can be simulated as the linear sum of contributions from warmer SSTs, direct radiative effects, and ozone changes. Second, we show that while surface warming induces ~85% of the BDC acceleration, its impact is limited to the lower stratosphere. By comparison, in the upper- and midstratosphere, the BDC response is dominated by changes due to direct radiative forcing from CO_2 (80% of the acceleration at 10 hPa). Third, we find that changes in ozone lead to a deceleration of the BDC, nearly canceling the acceleration by the CO_2 direct radiative forcing in the mid–lower stratosphere (30–70 hPa).

KEYWORDS: Dynamics; Stratospheric circulation; Climate models; Ozone

1. Introduvction

Recent studies have highlighted the importance of ozone adjustments in the atmosphere's response to increased carbon dioxide (CO_2). These adjustments, i.e., the changes in ozone caused by increasing concentrations of CO_2, may not only modulate climate sensitivity (Nowack et al. 2015; Marsh et al. 2016) but also the aspects of "dynamical sensitivity" (Grise and Polvani 2016), including the position and strength of the midlatitude eddy-driven jets (Chiodo and Polvani 2017; Chiodo et al. 2018), with potential impacts on the ocean circulation in both the Southern Hemisphere (Li and Newman 2023) and North Atlantic (Orbe et al. 2024). Typically, ozone adjustments act to reduce the response of the climate system to increased CO_2.

For example, Chiodo and Polvani (2017) show that ozone changes under $4 \times CO_2$ induce a weakening and equatorward shift of the tropospheric eddy-driven jet in the Southern Hemisphere (SH), which directly opposes the jet's well-known strengthening and poleward shift in response to increased CO_2 (Kushner et al. 2001; Barnes and Polvani 2013). In addition to the troposphere, Chiodo and Polvani (2019) hint at ozone having a significant impact on stratospheric circulation as well. This growing body of research suggests that, while not present in most climate models, ozone adjustments can substantially modify the atmospheric circulation's response to increased CO_2.

While previous studies have focused on the impacts of ozone adjustments on stratospheric temperatures and the SH tropospheric midlatitude jet, their impacts on the Brewer–Dobson circulation (BDC) have received less attention. This is despite growing evidence that the BDC response to climate change might be more complex than initially considered. In particular, while models consistently project an overall acceleration of the BDC with increasing CO_2 concentrations (Butchart et al. 2010), much uncertainty remains as to the vertical structure of this response, notably regarding which mechanisms may control the response of the shallow versus deep branches of the BDC (Abalos et al. 2021).

Previous studies have taken initial steps toward disentangling these mechanisms. Garny et al. (2011) first showed that an increase in stratospheric tropical upwelling in response to greenhouse gas forcing is primarily driven indirectly by tropical surface warming. Subsequently, Oberländer et al. (2013) identified that the direct radiative impact of greenhouse gases on the BDC is limited to the upper stratosphere. Following this line of inquiry, Chrysanthou et al. (2020) used an atmosphere-only model with independently prescribed sea surface temperatures (SSTs) and CO_2 concentrations to show that global surface warming drives 70% of the increase in mass

Supplemental information related to this paper is available at the Journals Online website: https://doi.org/10.1175/JCLI-D-25-0515.s1.

Corresponding author: Molly E. Menzel, molly.erin.menzel@gmail.com

DOI: 10.1175/JCLI-D-25-0515.1

TABLE 1. List of simulations included in the experimental design.

Configuration	Notation	CO_2	SST	O_3
Coupled	$piControl_{cpld}$	$1 \times CO_2$	Interactive	Interactive
	$(4 \times CO_2)_{cpld}$	$4 \times CO_2$	Interactive	Interactive
Atmosphere only	$piControl_{atmos}$	$1 \times CO_2$	$piControl_{cpld}$	$piControl_{cpld}$
	$(4 \times CO_2)_{atmos}$	$4 \times CO_2$	$(4 \times CO_2)_{cpld}$	$(4 \times CO_2)_{cpld}$
	$RAD^{4\times CO_2}_{atmos}$	$4 \times CO_2$	$piControl_{cpld}$	$piControl_{cpld}$
	$SST^{4\times CO_2}_{atmos}$	$1 \times CO_2$	$(4 \times CO_2)_{cpld}$	$piControl_{cpld}$
	$O_{3atmos}^{4\times CO_2}$	$1 \times CO_2$	$piControl_{cpld}$	$(4 \times CO_2)_{cpld}$

flux at 70 hPa under abrupt $4 \times CO_2$ forcing. In contrast, at 10 hPa, the role of direct radiative CO_2 cooling is comparable to the role of SSTs (Chrysanthou et al. 2020), highlighting the importance of the rapid adjustment of stratospheric temperatures in accelerating the deep branch of the BDC. With that said, stratospheric ozone was kept at preindustrial levels in all their simulations, so the role of ozone adjustments could not be evaluated in that study.

That role was originally noted in DallaSanta et al. (2021), who showed that ozone adjustments dampen the BDC acceleration in response to increased CO_2. However, that finding was somewhat incidental in their study which focused, rather, on the impacts of ozone adjustments on the quasi-biennial oscillation. In contrast, the more recent study of Hufnagl et al. (2023) focused explicitly on quantifying how ozone adjustments impact the BDC under abrupt $4 \times CO_2$ forcing. Comparing the BDC acceleration in an atmosphere-only model with and without concurrent ozone changes, they confirmed that the presence of interactive ozone dampens the BDC response to increased CO_2, by roughly 20% in their model. Both studies further showed that the damping of the BDC by ozone adjustments is vertically dependent, operating mainly between 15 and 40 hPa and below 20 hPa in DallaSanta et al. (2021) and Hufnagl et al. (2023), respectively.

Finally, in a recent paper, Calvo et al. (2025) examined the times scales of the response of the BDC to abrupt $4 \times CO_2$ forcing, comparing the fast and slow responses in two configurations of their model: a fully coupled configuration (i.e., with an interactive ocean component and progressively warming SSTs) and a fixed-SST atmosphere-only configuration (i.e., with prescribed preindustrial SSTs). They reported that both the shallow and the deep branches of the BDC respond on relatively fast time scales (i.e., within the two decades after CO_2 quadrupling) and confirmed the findings of Chrysanthou et al. (2020) that in the shallow branch, acceleration is dominated by the warming SSTs, while the direct radiative cooling of the stratosphere by CO_2 is important in the deep branch. Unlike Chrysanthou et al. (2020), however, the model employed by Calvo et al. (2025) included interactive ozone chemistry, so that the role of stratospheric ozone adjustments on the BDC response was indeed accounted for, although it could not be separately quantified.

In summary, these previous studies suggest that the BDC response to increased CO_2 is 1) vertically dependent 2) with different mechanisms controlling the responses of the deep and shallow branches and 3) sensitive to adjustments from ozone. These findings, however, have been obtained by independent groups working with models in somewhat different configurations. As such, a clean quantitative comparison of the relative importance of each mechanism, within a single and self-consistent model framework, is still lacking.

To this end, we here perform the first complete and consistent decomposition of the BDC response to abrupt CO_2 forcing into three distinct components: the direct radiative cooling of the stratosphere, the warming of the SSTs, and the changes of stratospheric ozone. We first run the model in a fully coupled configuration (i.e., with coupled atmosphere and ocean components and with prognostic ozone concentrations) subjecting the preindustrial climate state to an abrupt $4 \times CO_2$ forcing. Using this output, we then run the atmosphere-only model and demonstrate in section 2 that specifying the increased atmospheric CO_2 concentrations, warmer SSTs, and the ozone changes from the coupled configuration yields a nearly identical result. Having validated the decomposition, in section 3, we document and quantify the relative importance of each mechanism on key features of stratospheric circulation. A summary of our results is presented in section 4, together with some discussion.

2. Methodology and validation

a. *Model configurations and simulations*

In this study, we present output from seven simulations in two configurations of the NASA Goddard Institute for Space Studies model E2.2 (GISS-E2.2) "middle atmosphere" (Rind et al. 2020; Orbe et al. 2020), see Table 1. Relative to the lower-top GISS Coupled Model Intercomparison Project phase 6 (CMIP6) climate model submission, GISS-E2.2 was optimized for stratospheric processes through incorporation of higher vertical resolution, a higher model top, and a more complete parameterization of nonorographic gravity wave drag, leading to an interactive quasi-biennial oscillation.

The first configuration couples the model's atmosphere, ocean, sea ice, and land components. Two simulations use this coupled configuration: a control simulation, where all compositions are held at their preindustrial levels ($piControl_{cpld}$), and a climate change simulation, where the CO_2 is abruptly quadrupled and held constant for 150 years, denoted $(4 \times CO_2)_{cpld}$. For completeness, we show the resulting temperature changes in Figs. 1 and 2, where one can see the familiar stratospheric

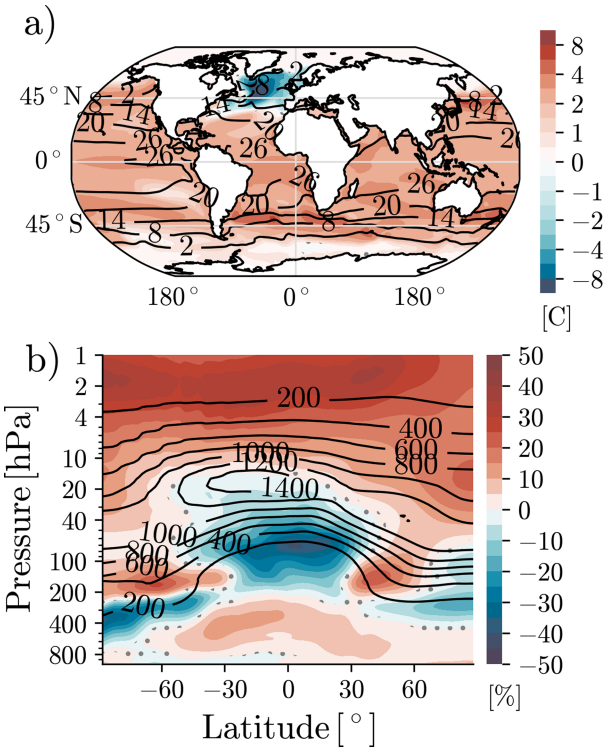

FIG. 1. Zonal-mean DJF climatology (black contours) and response (colored shading) to an abrupt $4 \times CO_2$ in the last 50 years of a 150-yr simulation of (a) SSTSs (C) and (b) ozone (DU). Note, the response of the ozone is shown relative to the climatological values.

cooling and tropospheric warming (Fig. 2a) and the global warming at the surface with the expected North Atlantic warming hole (Fig. 1a).

In both the control and perturbation simulations of this coupled climate configuration, ozone responds to CO_2 following the linearized ozone ("LINOZ") scheme, introduced by McLinden et al. (2000), such that the ozone tendency is, to first order, parameterized as a function of the local ozone mixing ratio, temperature, and overhead column ozone. In GISS-E2.2, the simplified LINOZ parameterization is applied throughout the whole atmosphere and has been shown to adequately produce the structure of ozone response resulting from a more comprehensive configuration with full interactive chemistry (DallaSanta et al. 2021). Particularly relevant for this study is that the LINOZ scheme accurately captures all the key features of the ozone's response to $4 \times CO_2$, notably the decrease in the tropical lower stratosphere and the increase in the upper stratosphere and in the polar regions (Fig. 1b). This pattern of ozone change with CO_2 is robust across various climate models (Chiodo et al. 2018; Hufnagl et al. 2023).

The second configuration of our model is used to perform the remaining five simulations: Here, only the atmospheric component is used, and it is forced with prescribed atmospheric composition and SSTs. The first two simulations mimic those performed with the coupled climate configuration. One is a control simulation ($\text{piControl}_{\text{atmos}}$) in which we hold both the atmospheric composition and the SSTs at their preindustrial values; the other is an abrupt climate change simulation $(4 \times CO_2)_{\text{atmos}}$ in which CO_2 is abruptly quadrupled and held constant, while the SSTs and ozone fields are prescribed from the $(4 \times CO_2)_{\text{cpld}}$ output. We emphasize that all other natural and anthropogenic forcings are kept at preindustrial values in all simulations.

The three remaining atmosphere-only simulations are designed to isolate the respective impacts of three key drivers under consideration: direct radiative CO_2 forcing, surface warming, and stratospheric ozone adjustments to increased CO_2. In each simulation, we prescribe drivers using the output from the $(4 \times CO_2)_{\text{cpld}}$, while holding the other drivers and all other forcings at their preindustrial levels. Specifically, to test the role of direct radiative CO_2 forcing, in the $\text{RAD}_{\text{atmos}}^{4\times CO_2}$ simulation, only CO_2 concentrations are abruptly quadrupled, while the SSTs and ozone are kept at their control values. And likewise, in the $\text{SST}_{\text{atmos}}^{4\times CO_2}$ and $O_{3\text{atmos}}^{4\times CO_2}$ simulations, we only prescribe the SSTs and the ozone from the $(4 \times CO_2)_{\text{cpld}}$ simulation, respectively, and keep everything else as in the $\text{piControl}_{\text{atmos}}$ simulation.

All model simulations analyzed in this paper are 150-yr long, and we emphasize that in each of the atmosphere-only simulations, the full transient structure of the individual drivers is prescribed from the corresponding coupled run. For instance, the $\text{SST}_{\text{atmos}}^{4\times CO_2}$ simulation is driven with the entire monthly time series of SSTs from the fully coupled simulation with quadrupled CO_2 levels and likewise for the prescribed ozone field in $O_{3\text{atmos}}^{4\times CO_2}$. Additionally, the prescribed fields are three-dimensional, varying in longitude as well as latitude and level, which impacts key circulation features (Albers and Nathan 2012; Ivanciu et al. 2021). Although one could simply use the zonal-mean steady-state response of SSTs and ozone to abrupt $4 \times CO_2$ forcing, as is done in Hufnagl et al. (2023), maintaining the zonal and transient structure of these fields allows us to precisely determine how faithfully the atmosphere-only model with prescribed SSTs and ozone is able to replicate the fully coupled response (see below).

While our atmosphere-only simulations were designed to maximally reproduce the coupled ones, for the sake of brevity, we have decided to focus here only on the "equilibrium" response. Such response is calculated as the difference between a forced simulation, averaged over the last 50 years, and its respective control run, averaged across the entire time series. Statistical significance is then determined using a 95% confidence interval two-tailed Student's t test. We denote the response of variable χ under forcing F as $\Delta_\chi F$, so, for instance, the response of ozone to quadrupled CO_2 in the fully coupled model is $\Delta_{O_3}(4 \times CO_2)_{\text{cpld}}$.

b. *Validation of the decomposition*

Before examining the individual impacts of direct radiative CO_2 forcing, SST warming, and ozone changes on the BDC, we seek to validate our methodology. The first step consists of determining to what degree the response to $4 \times CO_2$ forcing in the atmosphere-only model reproduces the fully coupled response when carbon dioxide, SSTs, and ozone from the fully

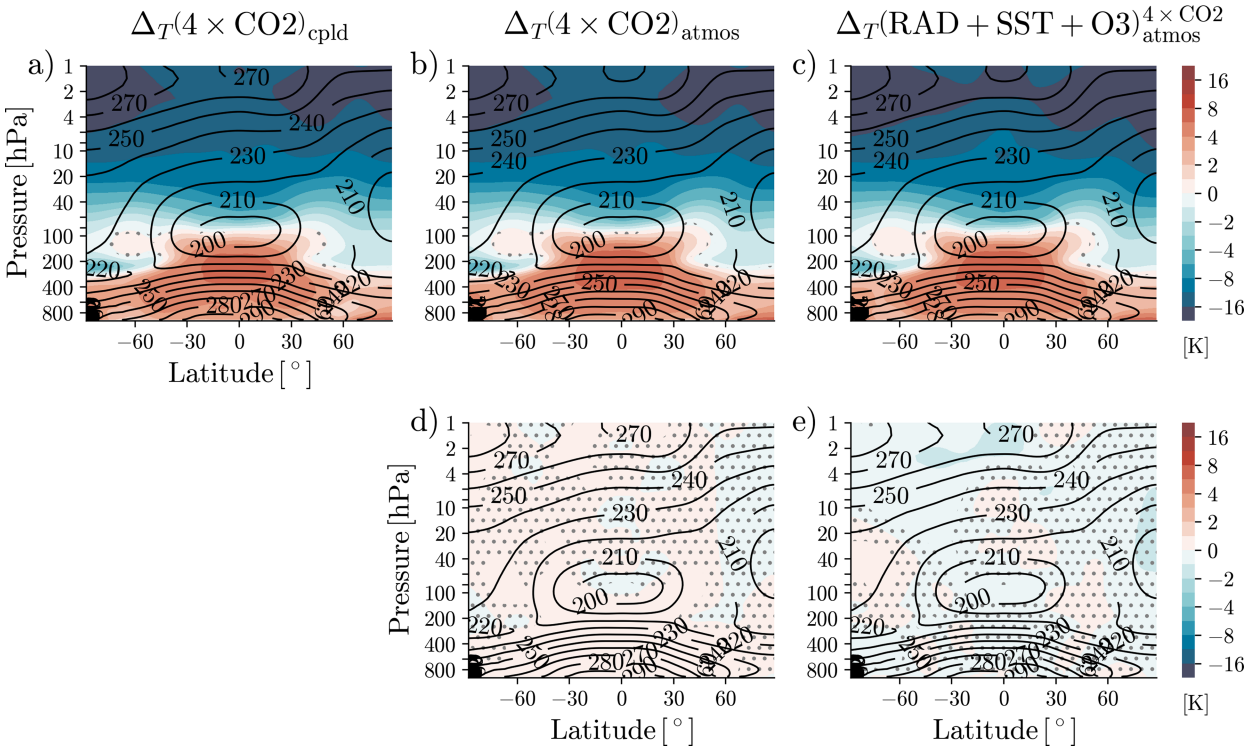

FIG. 2. Zonal-mean climatology (black contours) and response (colored shading) of the temperature T (K) for (a) $(4 \times CO_2)_{cpld}$, (b) $(4 \times CO_2)_{atmos}$, and (c) $(RAD + SST + O_3)^{4\times CO_2}_{atmos}$ for DJF. (d) The difference (b) − (a); (e) the difference (c) − (b). Stippling indicates the lack of statistical insignificance at the 95% level.

coupled model are prescribed in the atmosphere-only model. In other words, we seek to demonstrate that

$$\Delta_\chi(4 \times CO_2)_{cpld} \approx \Delta_\chi(4 \times CO_2)_{atmos}. \quad (1)$$

For the variables χ, we examine the atmospheric temperature T, the zonal wind u, and the residual mass streamfunction ψ^*, whose December–February (DJF) responses are shown in Figs. 2–4, respectively [see Figs. S2–S4 in the online supplemental material for the June–August (JJA) response]. Contrasting panels a and b in Figs. 2–4, it becomes clear that the atmosphere-only model configuration closely reproduces the atmosphere's response to CO_2 in the coupled model configuration.

Specifically, comparison of the atmosphere-only model response with that of the coupled model (Fig. 2d) shows that the former captures ~90% of the warming in the troposphere, including the well-known enhanced warming in the tropical upper troposphere and the enhanced warming over the Arctic in lower troposphere (Arctic amplification). It also captures ~98% of the strong cooling in the stratosphere that maximizes at about 2 hPa (Figs. 2a,b). The difference between $\Delta_T(4 \times CO_2)_{cpld}$ and $\Delta_T(4 \times CO_2)_{atmos}$, shown in Fig. 2d, is smaller than one degree nearly everywhere.

Additionally, the atmosphere-only model reproduces the strengthening of the polar vortex, the weakening of the stratospheric summer easterlies (see above 10 hPa between 30° and 80°S), the strengthening of the subtropical jets, and the poleward shift of the eddy-driven jet in both hemispheres (Figs. 3a,b). Again, the differences between coupled model and atmosphere-only model are much smaller than the response itself (Fig. 3d).

And, last, the atmosphere-only configuration yields the same notable changes in the meridional circulation as the coupled configuration, in particular the acceleration of the BDC in the winter hemisphere (Figs. 4a,b). Only minute differences can be seen—in the lowermost stratosphere—between the coupled and atmosphere-only response (Fig. 4d).

Despite an overall good agreement, the atmosphere-only configuration shows a subtly enhanced atmospheric circulation response to $4 \times CO_2$ in certain locations. Note, in particular, a relatively larger strengthening of the stratospheric polar vortex and upper-tropospheric subtropical zonal wind (Fig. 3d). It is possible that, since those responses come from averaging only five decades, some internal variability may lie behind the small discrepancies in the circulation response between the coupled and atmosphere-only configurations. The polar stratosphere in winter, in particular, is highly variable, and a different number of sudden warmings would be enough to produce such the difference we are seeing. Nonetheless, for the purposes of understanding the BDC response to CO_2 increases, we consider the differences minor and possibly the result of an interactive versus prescribed ozone field (Ivanciu et al. 2021). Also note that while our atmosphere-only configuration faithfully simulates the $4 \times CO_2$ response in the coupled configuration, the coupled model response is

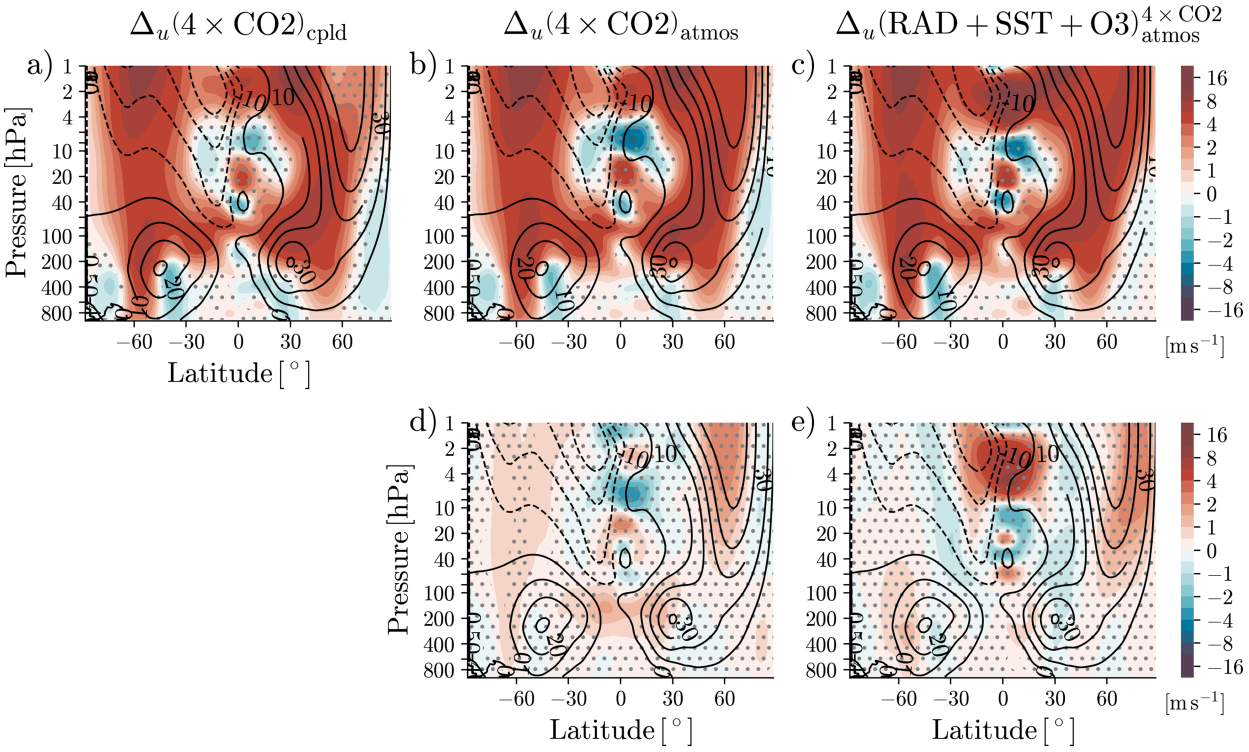

FIG. 3. As in Fig. 2, but for the zonal wind u (m s^{-1}).

likely to be somewhat model dependent. For instance, the notable strengthening of the polar vortex is not consistent across coupled climate models (Karpechko et al. 2022). The focus of our study is not to explain or even enumerate model-dependent results but rather to confirm the idealized configurations are representative of the coupled model in our simulation design.

Having established that the atmosphere-only model accurately reproduces the stratospheric response of the coupled model, we now need to address the question of additivity. In other words, before discussing the individual responses to the three key drivers that are the subject of this paper, we need to make sure that when the responses are individually computed

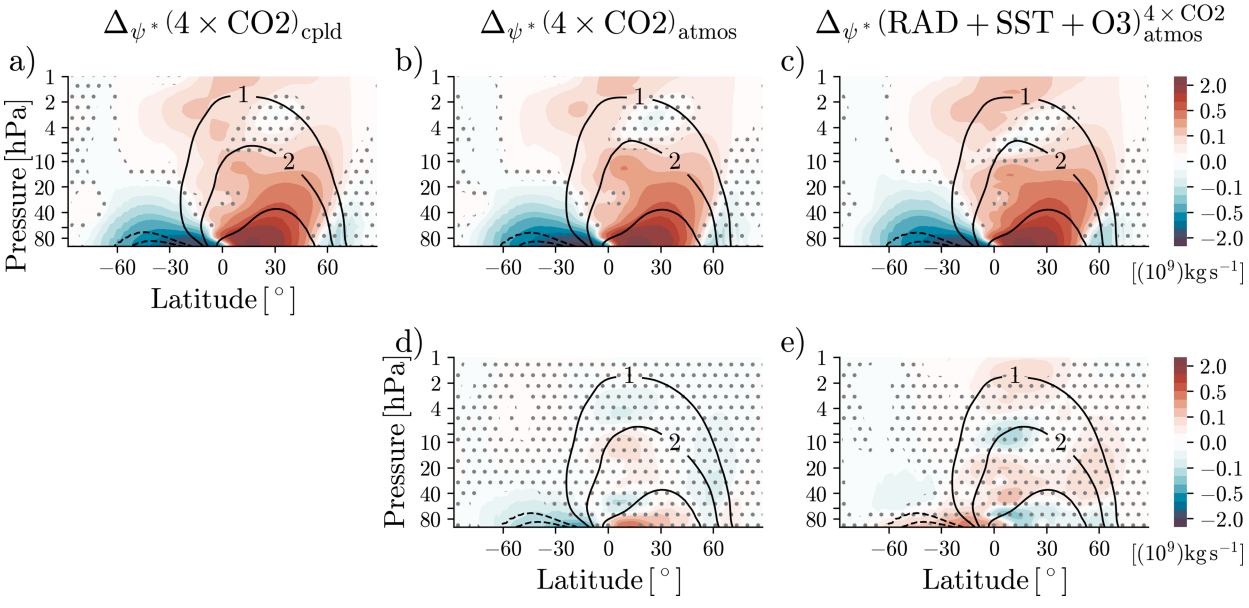

FIG. 4. As in Fig. 2, but for the stratospheric-mean residual streamfunction ψ^* (10^9 kg s^{-1}).

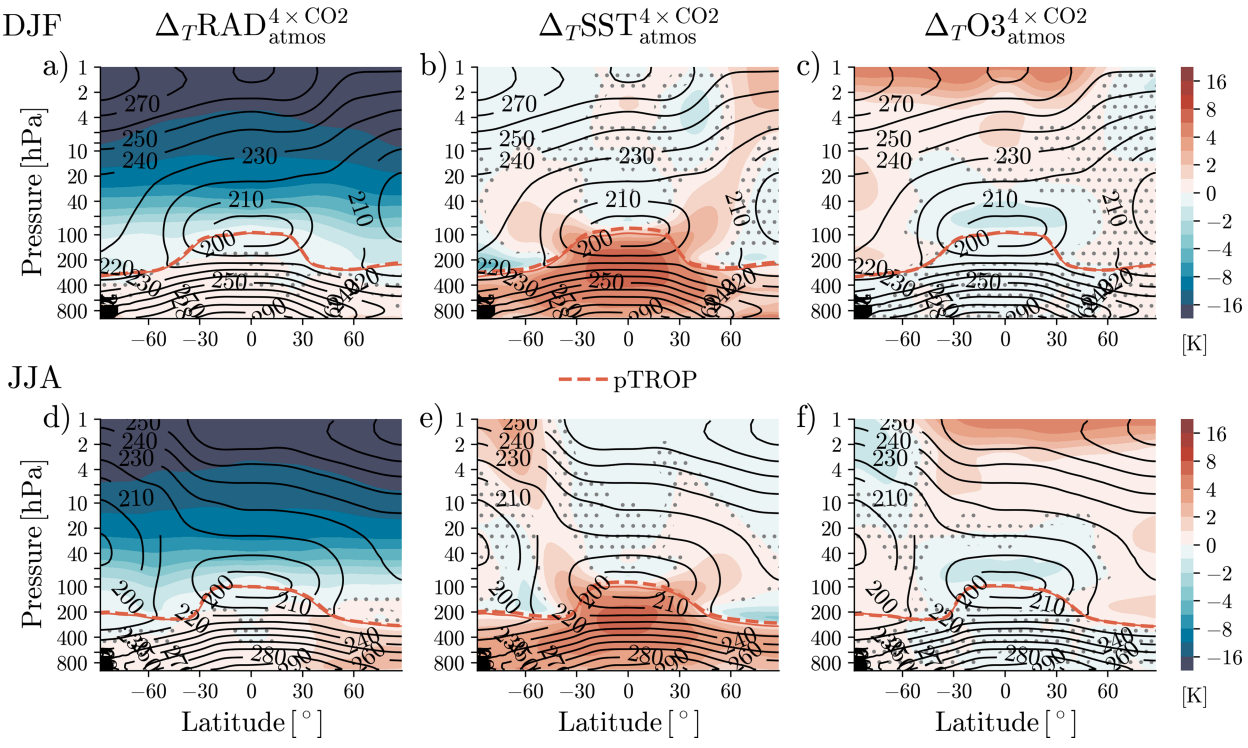

FIG. 5. Zonal-mean temperature response (colors) (K) to (left) $RAD^{4\times CO_2}_{atmos}$, (middle) $SST^{4\times CO_2}_{atmos}$, and (right) $O_{3\,atmos}^{4\times CO_2}$ forcing. (top) DJF and (bottom) JJA. Stippling indicates a statistically insignificant response at the 95% confidence interval. The solid contours show the climatological temperature field in the control simulation. The solid and dashed orange lines indicate the tropopause, in the control and the forced simulations, respectively.

in the atmosphere only-model and subsequently added together, their sum is similar to the one obtained by prescribing the drivers at the same time in the same model. That is, we seek to demonstrate that

$$\Delta_\chi(4\times CO_2)_{atmos} \approx \Delta_\chi RAD^{4\times CO_2}_{atmos} + \Delta_\chi SST^{4\times CO_2}_{atmos} + \Delta_\chi O_{3\,atmos}^{4\times CO_2}, \quad (2)$$

where χ stands, again, for one of T, u, or ψ^*. We emphasize that the validity of Eq. (2) has been implicitly assumed in previous studies (e.g., Chrysanthou et al. 2020; Hufnagl et al. 2023), whereas we here explicitly test it to validate the methodology.

As seen by contrasting panels b and c in Figs. 2–4, the response when the three drivers are specified together (panel b in Figs. 2–4) is very close to the sum of the responses to the three drivers specified individually (panel c in Figs. 2–4). This is confirmed by the fact that the differences between the right- and left-hand sides of Eq. (2)—shown in panel e of Figs. 2–4—are largely insignificant and likely due to internal variability. We, therefore, conclude that our methodology is sound, in the sense that the responses to the individual drivers (especially for the residual mass streamfunction) are robustly additive. Note, this additive nature may be a model-dependent result in of itself, and we advise its validation before the methodology is replicated in other models. Armed with this, we are now ready to discuss how the individual drivers affect the BDC under abrupt 4 × CO_2 forcing.

3. Decomposition of response

Now that we have confirmed the validity of our decomposition, we are ready to analyze the individual forcing simulations to compare in detail the relative impacts on the stratospheric circulation from the direct radiative CO_2 forcing, surface warming, and interactive ozone. It is useful to start by considering the temperature response to these forcings and the winds that are tied to temperature via thermal wind balance. As seen in Fig. 5, all three forcings impact stratospheric temperatures, but they do so in very different ways. The direct radiative CO_2 forcing accounts for nearly all stratospheric cooling and strongly increases with height from the tropopause to 1 hPa (Figs. 5a,d). In contrast, surface warming accounts for most of the tropospheric warming and also for considerable warming (1–3 K) in the stratosphere's mid–lower subtropics and midlatitudes and upper-level poles (Figs. 5b,e). As for ozone changes due to increased CO_2, while they induce a relatively smaller temperature response compared to the other forcings, they still have a significant impacts in both the tropical lower stratosphere, where they lead to cooling [as noted previously by Chiodo and Polvani (2019), Hufnagl et al. (2023)], and the upper stratosphere, where they lead to warming (Figs. 5c,f).

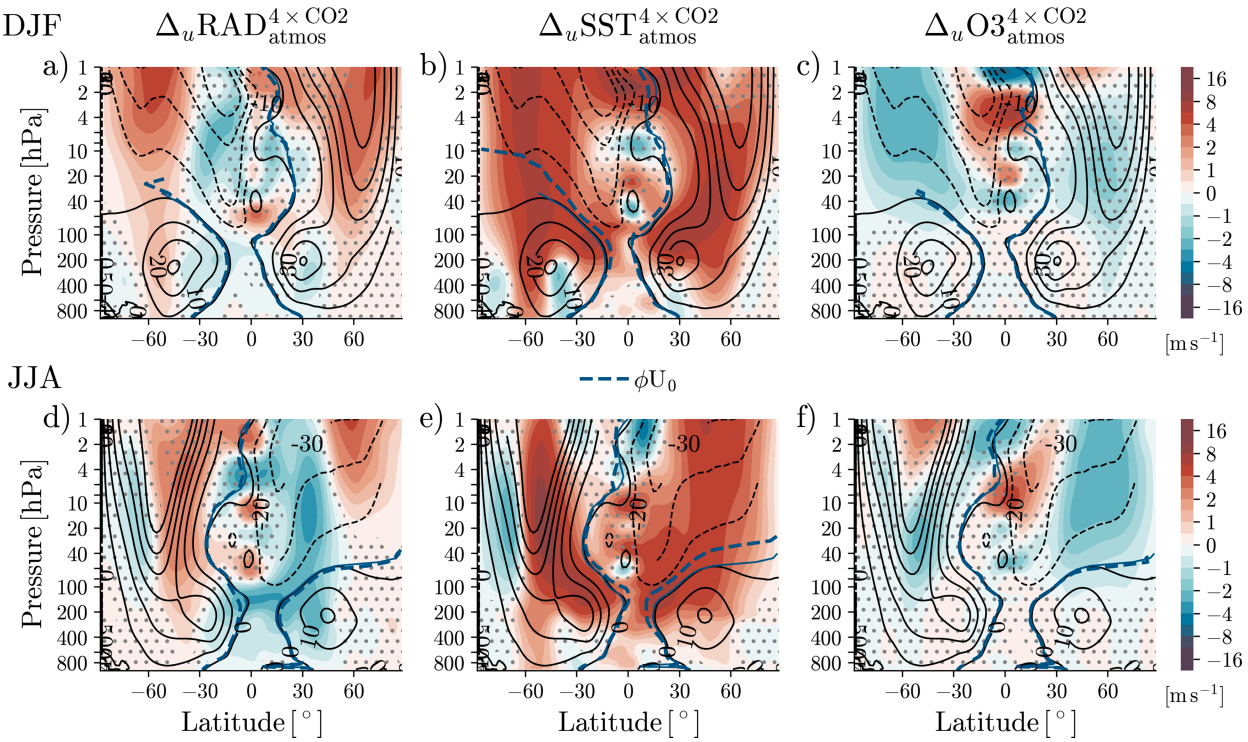

FIG. 6. As in Fig. 5, but for the zonal wind (u) (m s^{-1}). The solid and dashed blue lines indicate the critical latitude ($\phi_{U=0}$) for the control and the forced simulations, respectively.

As expected, the impacts of individual forcings on atmospheric temperature are associated with response patterns in the zonal winds. First, it is clear that the forcing from surface warming dominates the zonal winds' response, as seen in Fig. 6. It strengthens the stratospheric polar vortex by about 8–10 m s^{-1} in the midstratosphere (~10–40 hPa), strengthens the subtropical jet by a similar magnitude, shifts the tropospheric eddy-driven jet poleward, and reduces the summer easterlies (Figs. 6b,e). In the subtropical upper troposphere lower stratosphere (UTLS), these zonal wind responses are associated with an upward shift of the meridional temperature gradients (Figs. 7b,e): Between 30°S and 30°N and above 200 hPa, the upper flanks are enhanced and lower flanks are reduced. This overall pattern of change is consistent with a lifting of the tropopause (see discussion below) and associated with enhanced meridional temperature gradients in the subtropics between 40 and 100 hPa (Figs. 7b,e).

Second, the direct radiative CO_2 forcing also acts to strengthen the stratospheric polar vortex, albeit to a lesser degree (Figs. 6a,d). Unlike the surface warming, the direct radiative CO_2 forcing weakens the subtropical jet in JJA, and its impact on the summer easterlies is latitudinally dependent, characterized by a strengthening at lower latitudes and a weakening at higher latitudes. The weakening of the summer easterlies at higher latitudes is related to reduced meridional temperature gradients in the upper stratosphere (Figs. 7a,c). Since most of the meridional temperature gradients' response occurs higher in the stratosphere, only a minimal statistically significant response is seen at the 40–100-hPa level (Figs. 7a,d).

Third, interactive ozone affects the zonal wind response to quadrupled CO_2 concentrations, with larger seasonality that can also be connected to the meridional temperature gradients. Confirming the finding of Hufnagl et al. (2023), the summer easterlies strengthen in the extratropical lower stratosphere where the meridional temperature gradients are enhanced (Figs. 6 and 7c,f). Meanwhile, in the winter hemisphere, we see a slight weakening of the stratospheric polar vortex in extratropical midstratosphere, associated with reduced meridional temperature gradients in the same region, about 45°–60° above 100 hPa. Note that while we expect a strong relation between the responses of the zonal winds and meridional temperature gradients via thermal wind balance, our analysis does not imply any causality.

These changes in zonal wind are accompanied by changes in wave propagation that couples to the mean flow. To diagnose any connection, we consider the critical latitude ($\phi_{U=0}$) at which the zonal winds cross zero, as an approximation to the latitude of wave breaking (Hardiman et al. 2014). Most notably, we find that surface warming induces an equatorward and upward shift of $\phi_{U=0}$ in both seasons and in both hemispheres (see the blue lines in Figs. 6b,e). This shift in $\phi_{U=0}$ implies enhanced wave propagation at lower latitudes which could induce a BDC acceleration (Shepherd and McLandress 2011). In contrast, we find no significant response of $\phi_{U=0}$ for the other two forcings: Direct radiative CO_2 forcing might induce a slight poleward shift of $\phi_{U=0}$ (Figs. 6a,d), but change in $\phi_{U=0}$ due to the interactive ozone adjustment appears negligible (Figs. 6c,f). As a consequence, we conclude that any BDC response to direct radiative

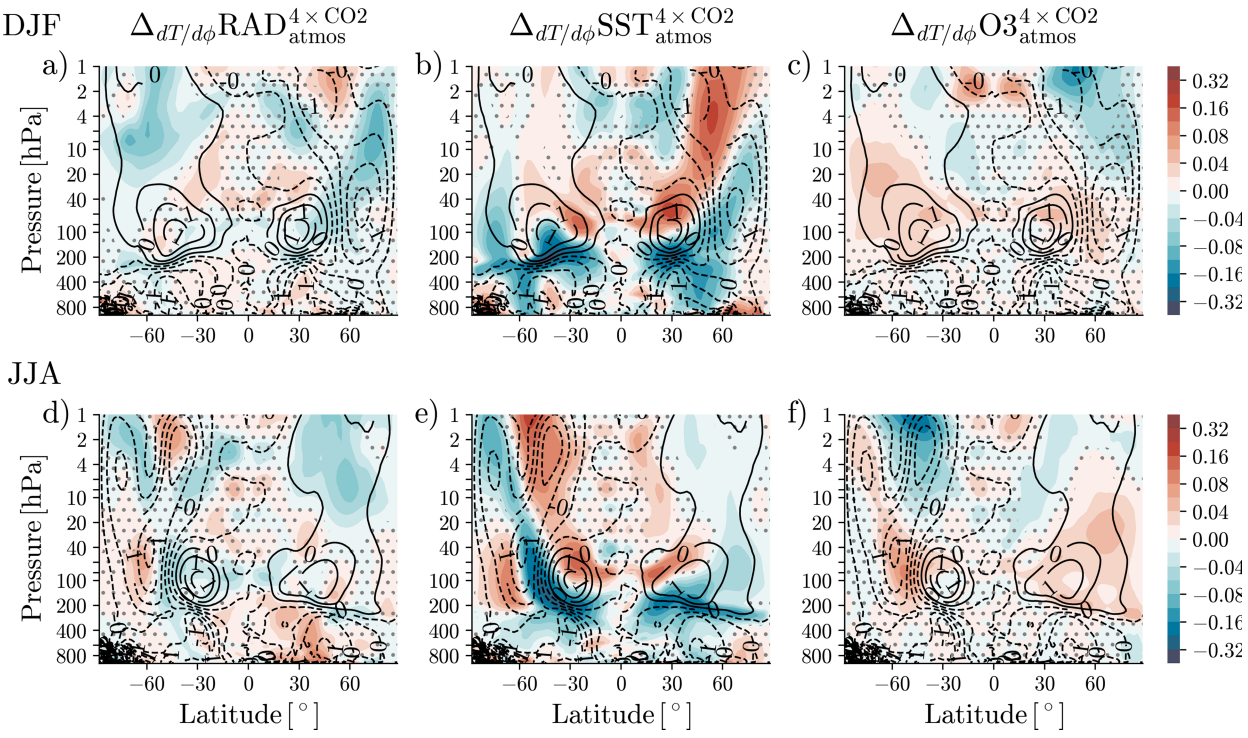

FIG. 7. As in Fig. 5, but for the meridional temperature gradient ($\partial T/\partial\phi$)(K N^{-1}). Positive and negative values denote poleward and equatorward increases in the gradient, respectively.

CO_2 forcing or interactive ozone simulations is unlikely to be related to the response of the subtropical UTLS zonal winds.

The computed BDC response itself, for each of the individual forcings, is shown in Fig. 8: It is clear that all three forcings contribute, but not all cause an acceleration. The direct radiative CO_2 forcing and surface warming induce a BDC acceleration but in very different ways. While the impact of surface warming is larger overall, it is confined to the lower stratosphere, below about 20 hPa (Figs. 8b,e). The direct radiative CO_2 forcing, instead, causes more uniform acceleration throughout the stratosphere (Figs. 8a,b).

In contrast to the changes due to direct radiative CO_2 forcing, CO_2-induced ozone changes weaken the residual meridional circulation (Figs. 8c,f). This weakening is statistically significant in both the summer and winter seasons and reaches into the midstratosphere to about 10 hPa. This key result—the deceleration of the BDC by the ozone changes associated with increased CO_2—provides an independent confirmation of the major finding of Hufnagl et al. (2023). In fact, our simulations show a slightly stronger statistical significance than theirs.

To better illustrate how the response of the circulation to the individual forcings relates to the width of the tropical upwelling region in the stratosphere, Fig. 8 also shows the turnaround latitudes of the residual-mean meridional streamfunction (ϕ_{TA}) (Rosenlof 1995), which delimit the tropical upwelling region. Most notably in response to surface warming, we note a slight narrowing of the upwelling in the lower stratosphere, consistent with the atmosphere's coupled response to 4 × CO_2 (Menzel et al. 2023). However, no significant narrowing or widening of the upwelling region is found for the other two forcings. These differing changes in the width of upwelling between the three perturbation simulations are consistent with the response of the critical latitudes shown in Fig. 6.

Next, we quantify how much of the residual streamfunction's strengthening may be reflective of tropospheric vertical expansion. Recall that since the tropopause rises in response to CO_2, a simple upward shift of the residual streamfunction would present a strengthening of the stratospheric circulation (Oberländer-Hayn et al. 2016). We explore this possibility by plotting the response of the tropopause pressure (p_T) to each of the forcings, see Fig. 9. Note the figure shows the response multiplied by −1 so that a positive change indicates an upward shift of the tropopause, and vice versa. As one might have guessed, the rising of the tropopause is largest under surface warming (Figs. 9b,e): p_T drops by about 10 hPa at nearly all latitudes except at 30°N/S where the tropopause climatologically slopes downward. The direct radiative CO_2 forcing also contributes to the rising of the tropopause, with a maximum impact in the subtropics (~10 hPa) and at higher latitudes (not shown). In both of these cases, the tropopause response (upward) is consistent with the response of the residual streamfunction (i.e., strengthening). However, this is not the case in response to interactive ozone. While latitudinally dependent, under ozone forcing, the tropopause rises in the tropics by about 2–4 hPa (Figs. 9c,f) even though this is accompanied by a weakening of the residual streamfunction in the tropical lower stratosphere.

To better calculate the residual streamfunction's sensitivity to the tropopause lifting, we transform the residual streamfunction

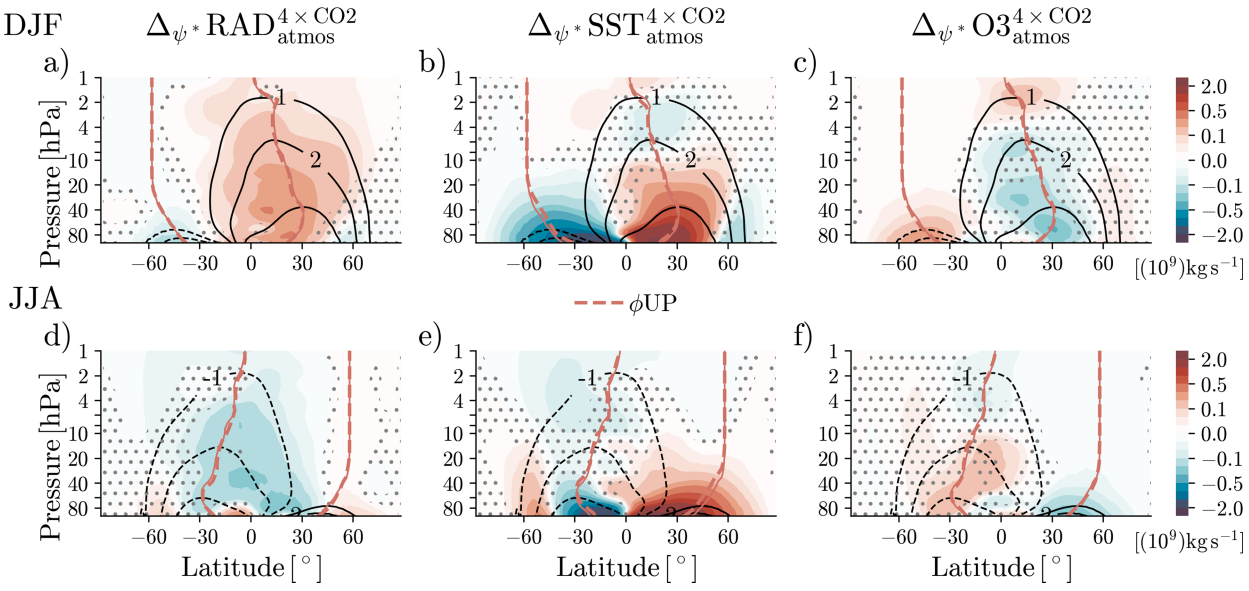

FIG. 8. As in Fig. 5, but for residual mass streamfunction (ψ^*) (10^9 kg s^{-1}). The solid and dashed pink lines indicate the turnaround latitudes (ϕ_{TA}) for the control and forced simulations, respectively.

according to that introduced by Singh and O'Gorman (2012) for zonal and meridional winds and subtract the climatological field. That is, we transform the meridional streamfunction as

$$\psi'(\phi, p, t) = \psi(\phi, \beta p, t), \tag{3}$$

where β is a scaling parameter such that $\beta > 1$ denotes an upward vertical shift. Instead of deriving the transformation's

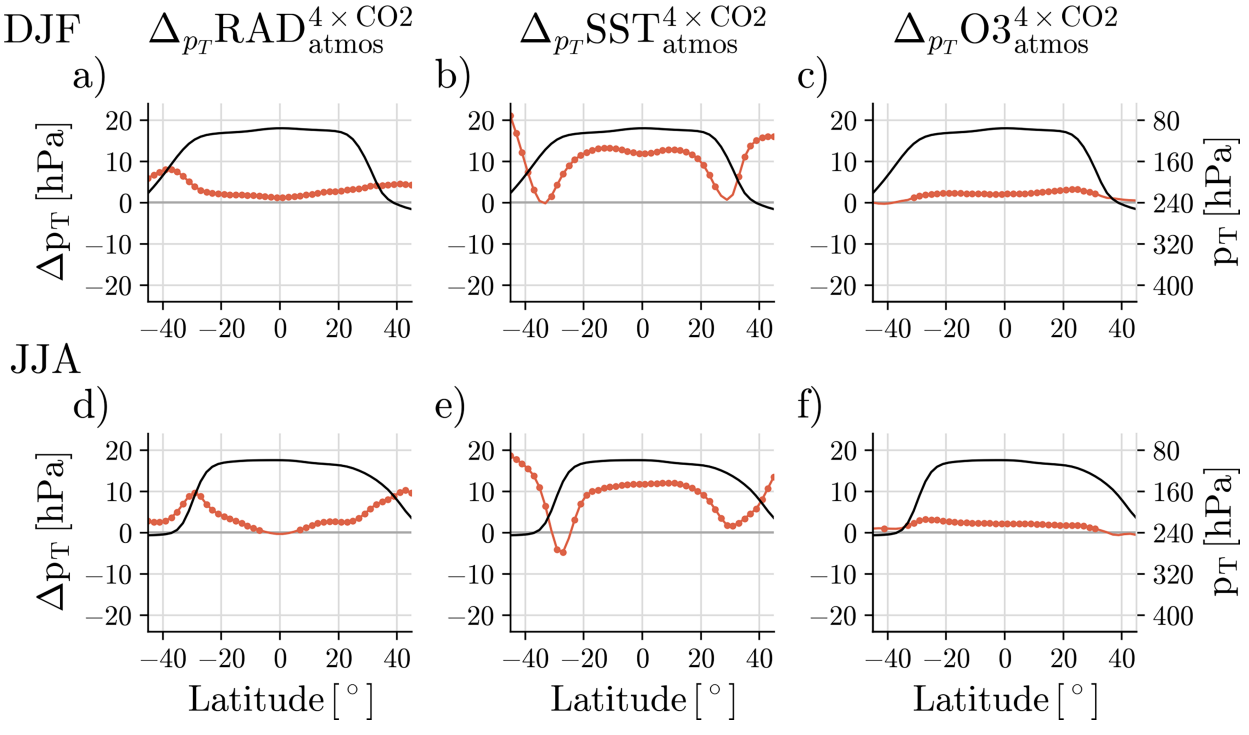

FIG. 9. As in Fig. 5, but for the tropopause pressure (p_T) (hPa). The red lines show the response, and the black lines show the climatology (with the ordinate axis to the right). Circles indicate statistical significance of the response at a 95% confidence interval. Note, the figure shows the response multiplied by −1 so that positive values indicate a rising of the tropopause.

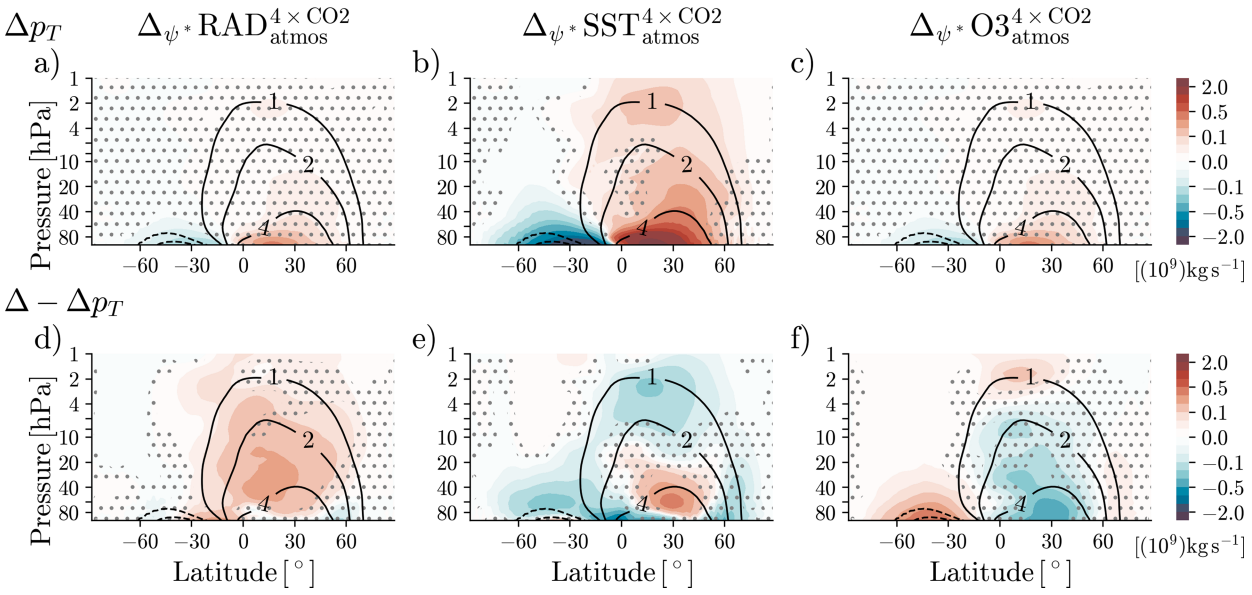

FIG. 10. Residual mass streamfunction response (colors) (10^{10} kg s^{-1}) to (left) $\mathrm{RAD}^{4\times\mathrm{CO}_2}_{\mathrm{atmos}}$, (middle) $\mathrm{SST}^{4\times\mathrm{CO}_2}_{\mathrm{atmos}}$, and (right) $\mathrm{O}_3{}^{4\times\mathrm{CO}_2}_{\mathrm{atmos}}$ forcing for DJF. (top) Response relative to the tropopause (p_T) and (bottom) the response insensitive to any tropopause shift. Stippling indicates statistical insignificance responses the 95% confidence interval. The solid contours show the climatological residual mass streamfunction field in the control simulation.

scaling number using a thermodynamic argument, as is done in Singh and O'Gorman (2012), we derive it via the change in tropopause pressure, presenting the tropopause-relative response. We then define the component of residual streamfunction response that is insensitive to the lifting of the tropopause as the residual between the tropopause-relative and total responses.

At first glance, the residual streamfunction's acceleration due to surface warming is significantly reflected in the upward shift of the tropopause (Fig. 10b). This is particularly true in the UTLS. Even so, the tropopause shift does not account for *all* of the residual streamfunction's response (Fig. 10e), which differs from the conclusion of Oberländer-Hayn et al. (2016). In contrast to surface warming, change in the tropopause pressure has a minimal and statistically insignificant impact on the residual streamfunction's response to both the direct radiative CO_2 forcing and the CO_2-induced ozone changes (Figs. 10a,c). We see this in how the component of response insensitive to the tropopause (Figs. 10d,f) well replicates that of the total response (Figs. 8a,c). Especially in the ozone perturbation simulation, the residual streamfunction's sensitivity to the tropopause opposes its overall response by driving an acceleration (Fig. 10c) rather than a weakening (Fig. 8c). Although Fig. 10 only presents the DJF response, results are consistent for JJA, see Fig. S6. We also find consistent results when considering the zonal-mean zonal wind (Figs. S7 and S8).

Finally, to quantify the strength of the BDC response at each level with a single number under each individual forcing, we evaluate the upwelling strength metric ψ^*_{max} (Menzel et al. 2023). At each pressure level, ψ^*_{max} is calculated as the sum of the absolute magnitude of the residual streamfunction at the turnaround latitudes ϕ_{TA}. The metric ψ^*_{max}, therefore, defines the residual streamfunction's magnitude using its extremum (Menzel et al. 2023). This metric is similar in nature to the upward mass flux diagnostic used by Rosenlof (1995).

Figure 11 shows the response of ψ^*_{max} under each individual forcing. The direct radiative CO_2 forcing induces a strengthening at all levels in the stratosphere; the response is largest in the mid–lower stratosphere, about 0.25 (10^9) kg s^{-1} up to 15 hPa (Figs. 11a,d). Similarly, surface warming induces a strengthening of ψ^*_{max} with a maximum value of 3 (10^9) kg s^{-1} in the lowermost stratosphere (Figs. 11b,e). Even though we see a small, albeit significant, impact above 5 hPa, the surface warming's predominant impact on the BDC strength is largely confined to below 20 hPa in DJF and below 40 hPa in JJA (Figs. 11b,e).

In contrast to the surface warming and CO_2 cooling, interactive ozone is found to reduce the BDC strength. Its impact is largest at about 70 hPa [approximately 0.5 (10^9) kg s^{-1}], but it extends as high as 6 hPa in DJF and 15 hPa in JJA (Figs. 11c,f). Additionally, the interactive ozone's impact is vertically dependent as it appears to increase ψ^*_{max} in the higher stratosphere, above 4 hPa.

The differences in how each individual forcing affects the BDC may be related to their impact on the zonal wind structure and thus the wave driving of the circulation. For instance, when considering the impact of surface warming, we showed above that the BDC's acceleration is associated with an equatorward and upward shift of $\phi_{U=0}$ and strengthening of the subtropical jet (Figs. 6b,e). These three signals are all consistent with changing wave propagation in the subtropical UTLS (Shepherd and McLandress 2011), and indeed, we find enhanced convergence of Eliassen–Palm (EP) fluxes in that region (Figs. 12b,e).

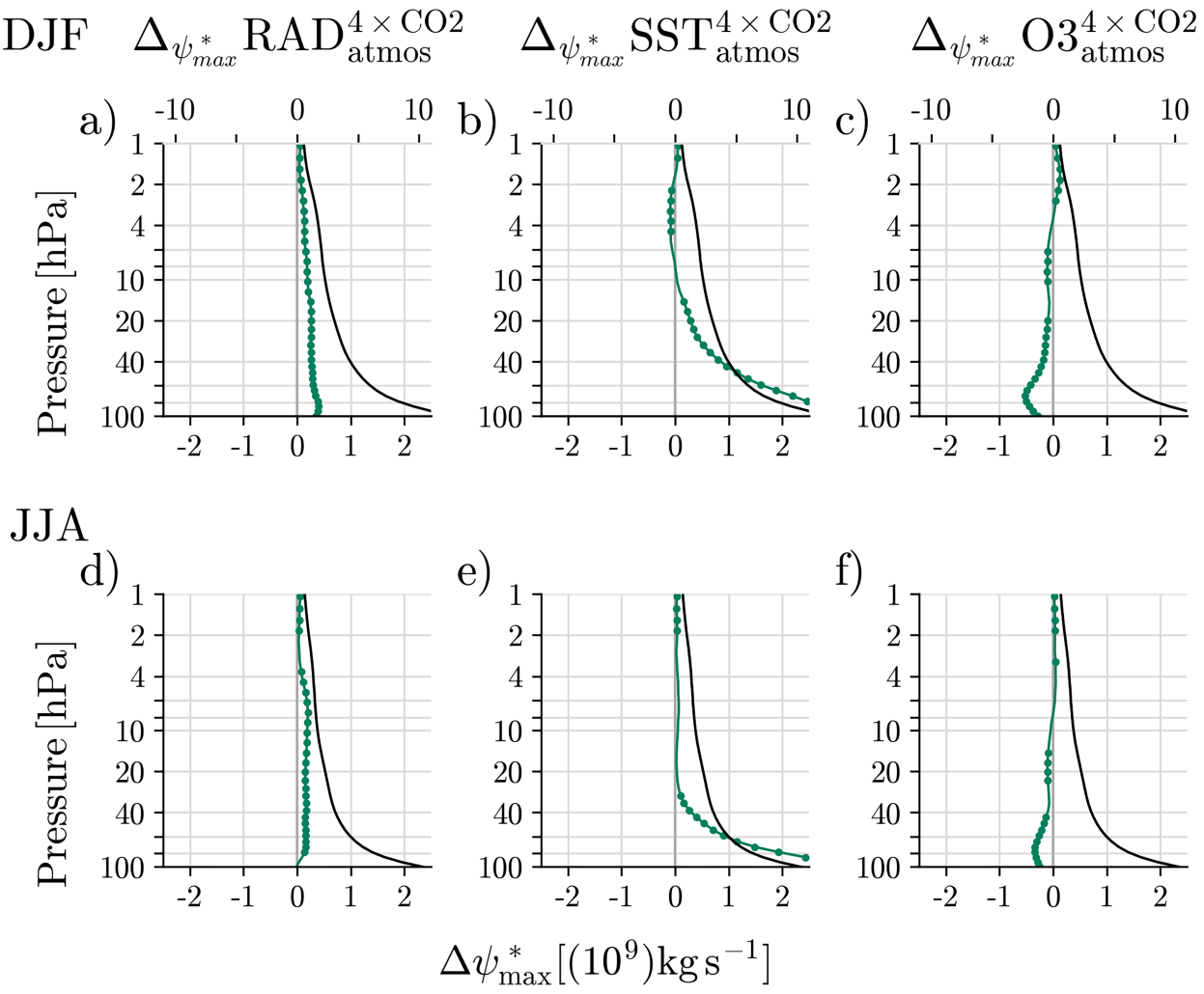

FIG. 11. As in Fig. 5, but for the zonal-mean BDC strength metric (ψ^*_{max}) (10^9 kg s^{-1}), with climatology in black and response in green. Circles indicate statistical significance at a 95% confidence interval.

However, the ozone changes have negligible impact on the subtropical UTLS zonal wind structure (Figs. 6c,f) and EP flux divergence (Figs. 12c,f), implying that the same mechanism cannot account for a reduction in the BDC by CO_2-induced ozone changes. Instead, the enhancement of the summer easterlies in the mid–upper stratosphere indicates a weakening of the westerlies or transitioning of westerlies to easterlies just below and is robust between our simulations and those in Hufnagl et al. (2023). These changes in the background zonal winds are accompanied by reduced convergence of the EP fluxes (Figs. 12c,f) and can influence the BDC via the downward control mechanism (Haynes et al. 1991). As a result, there is a slight lowering of the critical latitude in the summer midlatitudes even while there is no distinguishable change in critical latitude in the subtropical UTLS.

Likewise, the BDC response resulting from the direct radiative CO_2 forcing is inconsistent with changes in the subtropical UTLS zonal wind. Specifically in JJA, the BDC strengthening is accompanied by a weakening of the subtropical jets. There is also minimal change in EP fluxes in the lower stratosphere for both seasons (Figs. 12a,d). Although the exact mechanisms responsible for the BDC acceleration in response to the direct CO_2 radiative changes remain unclear, we can rule out UTLS dynamics as playing a key role.

The unique patterns of zonal wind response and wave driving to the three individual forcings are consistent across other models (Chrysanthou et al. 2020; Hufnagl et al. 2023) and indicate differing mechanisms at play for the different forcings. Brief inspection of changes in the wind tendencies due to resolved planetary waves (Fig. 12) versus gravity waves (Fig. S5) shows that the former clearly dominates over the latter in producing the zonal wind anomalies (Fig. 6). Specifically, interactive ozone induces a response of gravity waves that is nearly negligible in the summer hemisphere where the largest wind anomalies occur. This implication of resolved planetary wave changes is also consistent with the downward control analysis performed in Hufnagl et al. (2023, see their Figs. 8c,d).

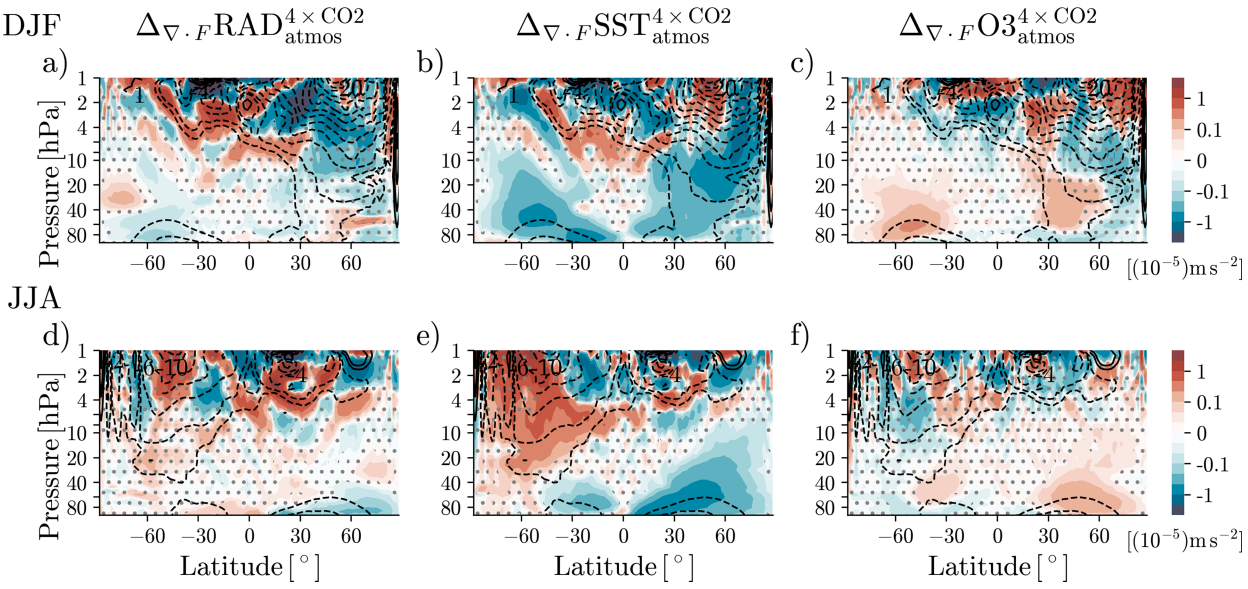

FIG. 12. As in Fig. 5, but for the EP flux divergence ($\nabla \cdot F$) (10^{-5} m s^{-2}).

4. Summary and discussion

The goal of this study has been to elucidate the pathways that lead to a strengthening of the BDC when CO_2 is increased. We decided to examine a simple large forcing (the abrupt quadrupling case) to avoid the complexities associated with more realistic future scenarios. Adopting a single-modeling framework to carefully analyze the response of the BDC to 4 × CO_2 forcing, we have focused on three largely independent mechanisms: the direct radiative cooling of the stratosphere, the warming of surface, and the chemical composition changes associated with the ozone layer. While these mechanisms are not strictly independent, they are easily separated given the model configurations currently available to us and can thus be independently quantified.

This quantification is presented in Fig. 13, where we summarize the key findings of our study, showing both percentage and absolute BDC responses in DJF (top tow) and JJA (bottom row). As in previous studies (Lin and Fu 2013), beyond the total response, we separately quantify the responses of the shallow and deep branches, and we also compute the response of transition branch in the UTLS. For each branch level, we calculate the BDC response as the change in ψ^*_{max} between the perturbation and respective control simulation, averaged over the corresponding stratospheric levels. We start by drawing attention to the fact that the atmosphere-only configuration well replicates the coupled-model response to 4 × CO_2: This is evidenced by the closeness of the black and gray bars in all panels of Fig. 13. We attribute the small differences to either internal variability (we are only averaging over 50 years at the end of each 4 × CO_2 run) or to very subtle nonlinear effects whose quantification one would be hard pressed to explore further.

Next, focusing on the colored bars in Fig. 13, we can draw several key conclusions. First, we see that the warming of the SSTs (red bars) is the main driver of BDC acceleration under 4 × CO_2 forcing. This result, which applies not only for the transition and shallow branches but also to the total BDC response, is far from obvious: If one thinks of the BDC as a fundamentally stratospheric circulation far away from the surface, one would not immediately guess that surface temperature changes are the main driver of the BDC response. Notice that, even in the deep branch, about 30%–40% of the changes are associated with surface warming.

Second, we see that the direct radiative cooling by CO_2 is the overwhelming driver of response in the deep branch, contributing more than 80% of the response there and in both seasons. However, since the BDC is a mass circulation, whereby the lower layers carry more weight, this direct radiative effect of CO_2 only contributes about a quarter to the total BDC acceleration.

We also note that the relative contributions of warmer SSTs and direct radiative CO_2 forcing found here are in excellent agreement with those reported in previous studies (Garny et al. 2011; Oberländer et al. 2013; Chrysanthou et al. 2020; Calvo et al. 2025). Quantitatively, Calvo et al. (2025) and Chrysanthou et al. (2020) independently found that surface warming accounts for 90% and 70% of enhanced upwelling in the UTLS, respectively.

Third, confirming previous studies (DallaSanta et al. 2021; Hufnagl et al. 2023), we find that ozone changes decelerate the BDC (blue bars in Fig. 13). While that effect is largely confined to the shallow and transition layers, it amounts to a total reduction of 15%–17%, which agrees well with a reduction of 20% found by Hufnagl et al. (2023). Similar damping of the circulation response to increased CO_2 driven by ozone changes caused by that CO_2 increase—an atmospheric composition feedback—has also been reported for the tropospheric circulation by Chiodo and Polvani (2017, 2019), although the mechanisms are likely to be quite different. Beyond presenting conclusions that confirm prior work, our quantification of the

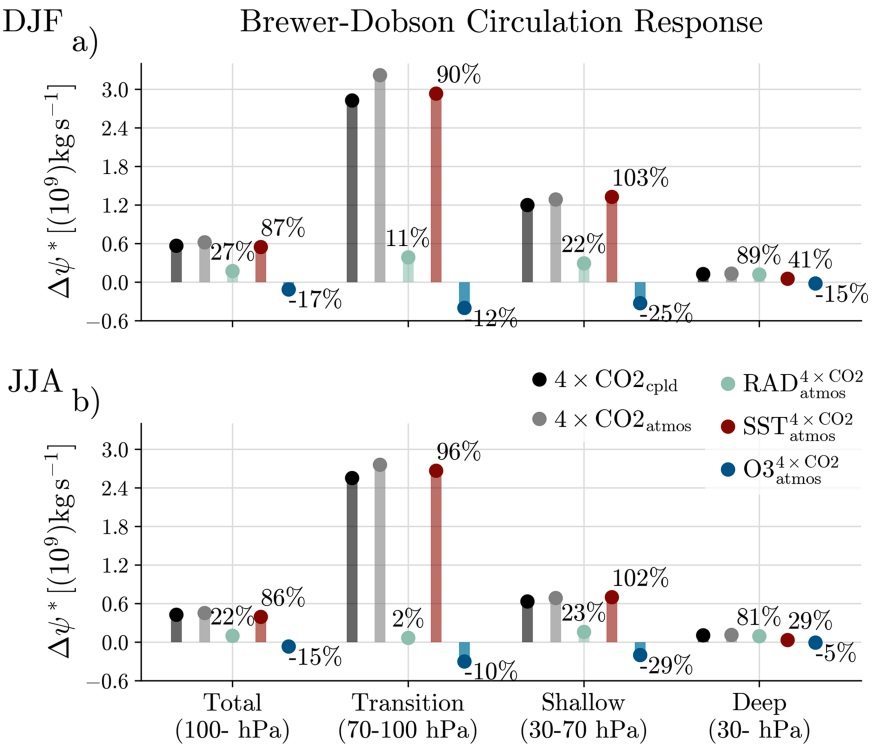

FIG. 13. Response of the BDC strength (10^9 kg s^{-1}) in $(4 \times CO_2)_{cpld}$ (black), $(4 \times CO_2)_{atmos}$ (gray), $RAD^{4\times CO_2}_{atmos}$ (green), $SST^{4\times CO_2}_{atmos}$ (red), and $O_3{}^{4\times CO_2}_{atmos}$ (blue), calculated for the total BDC (100 hPa and above), the transition layer (70–100 hPa), the shallow (30–70 hPa), and deep (30 hPa and above) branches. (top) DJF and (bottom) JJA. The relative contribution of individual forcings as a percentage of the $(4 \times CO_2)_{atmos}$ simulation is indicated as a percentage.

relative contributions of direct radiative CO_2, surface warming, and ozone changes is derived from a single-model framework, allowing for faithful comparison of the contributing factors.

Finally, the alert reader will have noticed that the percentages in Fig. 13 do not add to 100%. It may be worth keeping in mind that for a nonlinear, eddy-mediated, residual circulation such as the BDC, it would be naive to expect the response to the three drivers to be exactly additive. Nonetheless, our exercise allows us to quantify how far from linearly additive the response is. Remarkably enough, in both DJF and JJA, the total response is nearly completely additive and, even for the three different branches, the sum of the response to the three drivers is only 15% different from the response to the drivers specified together.

Needless to say, it would be of great interest to perform and analyze different model simulations with similar decomposition methodology as ours to assess the robustness of our results, in terms of the relative importance of each driver, and also vis-à-vis the additivity question. Unfortunately, the Coupled Model Intercomparison Project (CMIP) archive does not provide equivalent sets of experiments with other models, and thus, a clean separation cannot be performed. Nonetheless, the prescribed SST simulations (which are routine performed by the CMIP to compute effective radiative forcings) may be used to quantify the effect of surface warming on the BDC across a large number of models. Similarly, one might be able to explore the composition feedback from stratospheric ozone by grouping and contrasting CMIP simulations with and without interactive chemistry, as in Wang et al. (2025). Finally, we acknowledge that—while useful to ferret out specific mechanisms—the abrupt $4 \times CO_2$ forcing is not terribly realistic. Hence, exploration of future scenarios where forcing evolves in a transient fashion [e.g., the shared socioeconomic pathways, see Meinshausen et al. (2020)] would also be of much interest. Such work, however, is well beyond the scope of the present study.

Acknowledgments. Molly E. Menzel is grateful for collaboration with the International Space Science Institute (ISSI) in Bern, Switzerland, through ISSI International Team project 460, Tropical Width Impacts on the Stratosphere (TWIST). Molly E. Menzel was supported by an appointment to the NASA Postdoctoral Program at the Goddard Institute for Space Studies (GISS), administered by Oak Ridge Associated Universities under contract with NASA. LMP is funded, in part, by a grant from the U.S. National Science Foundation to Columbia University. Last, climate modeling at GISS is supported by the NASA Modeling, Analysis, and Prediction program, and resources supporting this work were provided by the NASA High-End Computing (HEC) Program through

the NASA Center for Climate Simulation (NCCS) at the Goddard Space Flight Center.

Data availability statement. The output from all simulations is publicly available via Zenodo (Menzel et al. 2025, https://doi.org/10.5281/zenodo.16993876).

REFERENCES

Abalos, M., and Coauthors, 2021: The Brewer–Dobson circulation in CMIP6. *Atmos. Chem. Phys.*, **21**, 13 571–13 591, https://doi.org/10.5194/acp-21-13571-2021.

Albers, J. R., and T. R. Nathan, 2012: Pathways for communicating the effects of stratospheric ozone to the polar vortex: Role of zonally asymmetric ozone. *J. Atmos. Sci.*, **69**, 785–801, https://doi.org/10.1175/JAS-D-11-0126.1.

Barnes, E. A., and L. Polvani, 2013: Response of the midlatitude jets, and of their variability, to increased greenhouse gases in the CMIP5 models. *J. Climate*, **26**, 7117–7135, https://doi.org/10.1175/JCLI-D-12-00536.1.

Butchart, N., and Coauthors, 2010: Chemistry–climate model simulations of twenty-first century stratospheric climate and circulation changes. *J. Climate*, **23**, 5349–5374, https://doi.org/10.1175/2010JCLI3404.1.

Calvo, N., R. R. Garcia, G. Chiodo, D. R. Marsh, and L. M. Polvani, 2025: On the timescales of the response of the Brewer-Dobson circulation to an abrupt quadrupling of CO_2. *J. Geophys. Res. Atmos.*, **130**, e2024JD041780, https://doi.org/10.1029/2024JD041780.

Chiodo, G., and L. M. Polvani, 2017: Reduced Southern Hemispheric circulation response to quadrupled CO_2 due to stratospheric ozone feedback. *Geophys. Res. Lett.*, **44**, 465–474, https://doi.org/10.1002/2016GL071011.

——, and ——, 2019: The response of the ozone layer to quadrupled CO_2 concentrations: Implications for climate. *J. Climate*, **32**, 7629–7642, https://doi.org/10.1175/jcli-d-19-0086.1.

——, ——, D. R. Marsh, A. Stenke, W. Ball, E. Rozanov, S. Muthers, and K. Tsigaridis, 2018: The response of the ozone layer to quadrupled CO_2 concentrations. *J. Climate*, **31**, 3893–3907, https://doi.org/10.1175/JCLI-D-17-0492.1.

Chrysanthou, A., A. C. Maycock, and M. P. Chipperfield, 2020: Decomposing the response of the stratospheric Brewer–Dobson circulation to an abrupt quadrupling in CO_2. *Wea. Climate Dyn.*, **1**, 155–174, https://doi.org/10.5194/wcd-1-155-2020.

DallaSanta, K., C. Orbe, D. Rind, L. Nazarenko, and J. Jonas, 2021: Dynamical and trace gas responses of the Quasi-Biennial Oscillation to increased CO_2. *J. Geophys. Res. Atmos.*, **126**, e2020JD034151, https://doi.org/10.1029/2020JD034151.

Garny, H., M. Dameris, W. Randel, G. E. Bodeker, and R. Deckert, 2011: Dynamically forced increase of tropical upwelling in the lower stratosphere. *J. Atmos. Sci.*, **68**, 1214–1233, https://doi.org/10.1175/2011JAS3701.1.

Grise, K. M., and L. M. Polvani, 2016: Is climate sensitivity related to dynamical sensitivity? *J. Geophys. Res. Atmos.*, **121**, 5159–5176, https://doi.org/10.1002/2015JD024687.

Hardiman, S. C., N. Butchart, and N. Calvo, 2014: The morphology of the Brewer–Dobson circulation and its response to climate change in CMIP5 simulations. *Quart. J. Roy. Meteor. Soc.*, **140**, 1958–1965, https://doi.org/10.1002/qj.2258.

Haynes, P. H., M. E. McIntyre, T. G. Shepherd, C. J. Marks, and K. P. Shine, 1991: On the "downward control" of extratropical diabatic circulations by eddy-induced mean zonal forces. *J. Atmos. Sci.*, **48**, 651–678, https://doi.org/10.1175/1520-0469(1991)048<0651:OTCOED>2.0.CO;2.

Hufnagl, L., R. Eichinger, H. Garny, T. Birner, A. Kuchař, P. Jöckel, and P. Graf, 2023: Stratospheric ozone changes damp the CO_2-induced acceleration of the Brewer–Dobson circulation. *J. Climate*, **36**, 3305–3320, https://doi.org/10.1175/JCLI-D-22-0512.1.

Ivanciu, I., K. Matthes, S. Wahl, J. Harlaß, and A. Biastoch, 2021: Effects of prescribed CMIP6 ozone on simulating the Southern Hemisphere atmospheric circulation response to ozone depletion. *Atmos. Chem. Phys.*, **21**, 5777–5806, https://doi.org/10.5194/acp-21-5777-2021.

Karpechko, A. Y., and Coauthors, 2022: Northern Hemisphere stratosphere-troposphere circulation change in CMIP6 models: 1. Inter-model spread and scenario sensitivity. *J. Geophys. Res. Atmos.*, **127**, e2022JD036992, https://doi.org/10.1029/2022JD036992.

Kushner, P. J., I. M. Held, and T. L. Delworth, 2001: Southern Hemisphere atmospheric circulation response to global warming. *J. Climate*, **14**, 2238–2249, https://doi.org/10.1175/1520-0442(2001)014<0001:SHACRT>2.0.CO;2.

Li, F., and P. A. Newman, 2023: Prescribing stratospheric chemistry overestimates Southern Hemisphere climate change during austral spring in response to quadrupled CO_2. *Climate Dyn.*, **61**, 1105–1122, https://doi.org/10.1007/s00382-022-06588-4.

Lin, P., and Q. Fu, 2013: Changes in various branches of the Brewer–Dobson circulation from an ensemble of chemistry climate models. *J. Geophys. Res. Atmos.*, **118**, 73–84, https://doi.org/10.1029/2012JD018813.

Marsh, D. R., J.-F. Lamarque, A. J. Conley, and L. M. Polvani, 2016: Stratospheric ozone chemistry feedbacks are not critical for the determination of climate sensitivity in CESM1(WACCM). *Geophys. Res. Lett.*, **43**, 3928–3934, https://doi.org/10.1002/2016GL068344.

McLinden, C. A., S. C. Olsen, B. Hannegan, O. Wild, M. J. Prather, and J. Sundet, 2000: Stratospheric ozone in 3-D models: A simple chemistry and the cross-tropopause flux. *J. Geophys. Res.*, **105**, 14 653–14 665, https://doi.org/10.1029/2000JD900124.

Meinshausen, M., and Coauthors, 2020: The shared socio-economic pathway (SSP) greenhouse gas concentrations and their extensions to 2500. *Geosci. Model Dev.*, **13**, 3571–3605, https://doi.org/10.5194/gmd-13-3571-2020.

Menzel, M. E., D. W. Waugh, and C. Orbe, 2023: Connections between upper tropospheric and lower stratospheric circulation responses to increased CO_2. *J. Climate*, **36**, 4101–4112, https://doi.org/10.1175/JCLI-D-22-0851.1.

——, C. Orbe, and L. Polvani, 2025: Distinguishing the direct radiative, surface warming, and ozone mediated contributions to the acceleration of the Brewer-Dobson circulation under abrupt CO_2 forcing. Zenodo, https://doi.org/10.5281/zenodo.16993876.

Nowack, P. J., N. L. Abraham, A. C. Maycock, P. Braesicke, J. M. Gregory, M. M. Joshi, A. Osprey, and J. A. Pyle, 2015: A large ozone-circulation feedback and its implications for global warming assessments. *Nat. Climate Change*, **5**, 41–45, https://doi.org/10.1038/nclimate2451.

Oberländer, S., U. Langematz, and S. Meul, 2013: Unraveling impact factors for future changes in the Brewer-Dobson circulation. *J. Geophys. Res. Atmos.*, **118**, 10 296–10 312, https://doi.org/10.1002/jgrd.50775.

Oberländer-Hayn, S., and Coauthors, 2016: Is the Brewer-Dobson circulation increasing or moving upward? *Geophys. Res. Lett.*, **43**, 1772–1779, https://doi.org/10.1002/2015GL067545.

Orbe, C., and Coauthors, 2020: GISS model E2.2: A climate model optimized for the middle atmosphere—2. Validation of large-scale transport and evaluation of climate response. *J. Geophys. Res. Atmos.*, **125**, e2020JD033151, https://doi.org/10.1029/2020JD033151.

——, D. Rind, D. W. Waugh, J. Jonas, X. Zhang, G. Chiodo, L. Nazarenko, and G. A. Schmidt, 2024: Coupled stratospheric ozone and Atlantic meridional overturning circulation feedbacks on the Northern Hemisphere midlatitude jet response to 4xCO_2. *J. Climate*, **37**, 2897–2917, https://doi.org/10.1175/JCLI-D-23-0119.1.

Rind, D., and Coauthors, 2020: GISS model E2.2: A climate model optimized for the middle atmosphere—Model structure, climatology, variability, and climate sensitivity. *J. Geophys. Res. Atmos.*, **125**, e2019JD032204, https://doi.org/10.1029/2019JD032204.

Rosenlof, K. H., 1995: Seasonal cycle of the residual mean meridional circulation in the stratosphere. *J. Geophys. Res.*, **100**, 5173–5191, https://doi.org/10.1029/94JD03122.

Shepherd, T. G., and C. McLandress, 2011: A robust mechanism for strengthening of the Brewer–Dobson circulation in response to climate change: Critical-layer control of subtropical wave breaking. *J. Atmos. Sci.*, **68**, 784–797, https://doi.org/10.1175/2010JAS3608.1.

Singh, M. S., and P. A. O'Gorman, 2012: Upward shift of the atmospheric general circulation under global warming: Theory and simulations. *J. Climate*, **25**, 8259–8276, https://doi.org/10.1175/JCLI-D-11-00699.1.

Wang, J., and Coauthors, 2025: Exploring ozone-climate interactions in idealized CMIP6 DECK experiments. EGUsphere, https://doi.org/10.5194/egusphere-2025-340.